Multibody Syst Dyn
https://doi.org/10.1007/s11044-020-09724-2

Active isotropic compliance in redundant manipulators

Matteo Verotti[1] · **Pierangelo Masarati**[2] · **Marco Morandini**[2] · **Nicola P. Belfiore**[3]

Received: 11 May 2019 / Accepted: 16 January 2020

Abstract The isotropic compliance property is examined in the Special Euclidean Group SE(3) in the case of redundant manipulators. The redundancy problem is solved by means of the QR decomposition of the transposed Jacobian matrix, and the compliance property is achieved by means of active stiffness regulation. Thanks to the defined control matrices, the control system realizes the isotropy condition. The local optimization of the joint torques is discussed. In particular, the joint control torques work is minimized obtaining an analytic solution through a Lyapunov equation. The proposed approach is applied to a 7R and to a 9R serial manipulator, and verified by means of multibody dynamics simulations.

Keywords Isotropic Compliance · Stiffness Matrix · Redundancy · QR decomposition · Torque minimization

1 Introduction

In the last decades, many investigations were conducted to improve the kinematic performance of manipulators [1–6], and the Jacobian matrix has been widely considered a key tool to evaluate these performance. For example, Yoshikawa defined the concept of *manipulability* as the square root of the determinant of the product of the Jacobian by its transpose [7], whereas Salisbury and Craig [8] introduced a performance index based on the Jacobian condition number. They introduced also the concept of *isotropic point*: a point of the workspace where the Jacobian matrix becomes *isotropic*, i.e. its condition number becomes equal to unity. Isotropy has been also discussed in the case of parallel manipulators [9, 10], and extended to various manipulator properties, such as force, stiffness, even repeatability and mass [11].

✉ M. Verotti
matteo.verotti@unige.it

1 Department of Mechanical, Energy, Management and Transportation Engineering, University of Genoa, 16145 Genoa, Italy

2 Dipartimento di Scienze e Tecnologie Aerospaziali, Politecnico di Milano, 20156 Milano, Italy

3 Department of Engineering, University of Roma Tre, 00146 Rome, Italy

Published online: 23 January 2020

The concept of *isotropic compliance* was initially introduced in $E(3)$ and achieved by means of active joint stiffness regulation [12, 13]. When this property is verified, the end-effector displacement is parallel to the applied force. The basic condition for the achievement of this property lies on the manipulator compliance matrix, $\mathbf{C}$, defined in the task space, which has to be a scalar matrix. More specifically, this property implies $\mathbf{C} = \mathbf{J}\mathbf{k}^{-1}\mathbf{J}^T = \lambda\mathbf{I}$, where $\mathbf{J}$ is the Jacobian matrix, $\mathbf{k}$ is the joint stiffness matrix, λ is a scalar and $\mathbf{I}$ is the identity matrix. Generally, matrix $\mathbf{k}$ originates from the passive compliance of the joints. Therefore, $\mathbf{k}$ is a diagonal matrix, but its elements are not necessarily equal. However, a control loop could be implemented, which makes the off-diagonal elements no longer null. This consideration, indeed, gave rise to the concept of *isotropic compliance*, which basically differs from *kinematic isotropy*. In fact, considering the singular values of $\mathbf{J}$, a serial non-redundant manipulator is defined isotropic when its Jacobian matrix satisfies the relation $\mathbf{J}\mathbf{J}^T = \lambda\mathbf{I}$ [6, 14]. Therefore, kinematic isotropy implies isotropic compliance only if all the joints have the same stiffness, i.e. $\mathbf{k}$ is a scalar matrix. As a consequence, the range of applications of the isotropic compliance is wider than the one related to kinematic isotropy: the former refers to manipulators characterized by a non-scalar stiffness matrix, the latter to manipulators with scalar stiffness matrix (all joints with equal stiffness value).

The feasibility of the isotropic compliance property was investigated in Ref. [15], where a workspace classification was proposed considering different types of isotropic compliance subsets. Therefore, isotropic compliance was extended to the Special Euclidean Group $SE(3)$, considering the relation between the wrench applied to the end-effector and the resulting twist [16]. In particular, two properties were introduced: *local* isotropic compliance, verified if the force vector and the torque axis are parallel to the end-effector displacement vector and to the rotation axis, respectively, and *screw* isotropic compliance, verified if the wrench screw axis is parallel to the twist screw axis. In the latter case, wrench and twist screw axes are in general parallel but not coincident. For this reason, two particular cases were considered: *task* screw isotropic compliance, verified if the screw axes are coincident, and *tool* screw isotropic compliance, verified if the common screw axis passes through the end-effector contact point. Two arrangements have been taken into account in Ref. [16] for the control system, operating either in parallel or as a series with the passive joint stiffness. The investigation was limited to a 6-DoF manipulator, therefore redundancy was not considered.

Generally, the capability of controlling the compliance response of a manipulator represents an opportunity that has been adopted in several systems [17]. For example, the compliance behavior of a finger of a *robogami* has been modeled and then controlled along different directions with both simulations and experiments [18]. A further example of the capability of controlling compliance along different directions has been also provided to synthesize compliance in a microgripper [19]. Finally, a compliance adaptation method has been also proposed to optimize the performance of robots employed in cyclic tasks [20] with the purpose of minimizing actuation forces and energy. Interestingly, the latter goal can be pursued also in the rather different case of redundant driven parallel manipulators, sometimes with a significant reduction of energy consumption [21].

In fact, redundancy can be used to meet user-defined tasks or additional constraints on the kinematic or dynamic control problem, such as obstacles [22–24] or joint–drift [25] avoidance, joint limitations [26–28], singularity avoidance [29, 30], energy saving optimization [31–33], torque [34–37] and antagonistic stiffness [38] optimization, force or torque control [39–42], impact force reduction [43], collision safety evaluation [44], to name the most relevant ones.

Many solutions have been proposed for the kinematic control problem of redundant manipulators, such as simple Jacobian-based techniques, gradient projection method, task-space augmentation, inverse kinematic functions [45], and quadratic programs-based optimization schemes [46].

Simple Jacobian-based techniques focus on the solution of the equation $\dot{\boldsymbol{s}} = \mathbf{J}\dot{\boldsymbol{q}}$, where $\boldsymbol{q}$ and $\boldsymbol{s}$ are the vectors of joint and task variables, respectively. The joint velocities vector $\dot{\boldsymbol{q}}$ is determined by considering a suitable control matrix based on the Jacobian, such as the Moore–Penrose pseudoinverse [47] or the damped least-square inverse [48] of $\mathbf{J}$. Other solutions consider the Jacobian transpose [49].

The gradient projection method generalizes the pseudoinverse minimum-norm solution by adding a homogeneous term defined by a projection operator. Such operator projects an arbitrary joint velocity vector $\dot{\boldsymbol{q}}_0$ in the nullspace of $\mathbf{J}$, therefore $\dot{\boldsymbol{q}}_0$ produces only internal motions. The vector $\dot{\boldsymbol{q}}_0$ is usually determined by optimizing a cost function related to, for example, joint range availability, obstacle avoidance, actuator energy consumption, torque and acceleration minimization, or other various criteria [45, 49, 50].

Considering the task-space augmentation method, a suitable constraint task is added to the end-effector task [51], whereas the inverse kinematic function approach consists in finding an inverse kinematic function on a workspace subset and in defining some optimization criteria [52].

Quadratic programs-based optimization schemes have been recently implemented to solve inequality and repeatability problems related to the constraints imposed by the system or the environment. Generally, these problems can be solved by means of numerical methods or neural networks, the latter based on parallel processing [53, 54].

Solving the inverse dynamics problem of redundant manipulators, formulated in the redundant coordinate set approach that is typical of modern multibody dynamics, has been recently addressed in Ref. [42].

In the present investigation, the isotropic compliance property is extended to the case of serial redundant manipulators. With respect to the previous investigation in $SE(3)$ [16], an optimization procedure is presented to solve the redundancy problem. More specifically, the proposed method is based on the QR decomposition of the transposed Jacobian matrix and on the minimization of the joint control torques work. An analytic solution is obtained through the Lyapunov matrix equation. Then proper control stiffness matrices are determined in the joint space.

In the present investigation, the isotropic compliance property is extended to the case of serial redundant manipulators. With respect to the previous investigation in $SE(3)$ [16], an optimization procedure is presented to solve the redundancy problem. The proposed method is based on the Jacobian transpose and on the minimization of the joint control torques work. More specifically, the novelty of this contribution lies on:

- the implementation of the QR decomposition for the transposed Jacobian matrix;
- the definition of the matrix $\boldsymbol{\gamma}$ for the minimization of the cost function;
- the analytical solution obtained through a Lyapunov algebraic matrix equation.

Then, proper control stiffness matrices are determined in the joint space.

The paper is organized as follows. In Sect. 2, the isotropic compliance problem is described and motivated; in Sect. 3, some basic concepts of the redundancy problem are recalled, whereas in Sect. 4 and the solution strategy is described. In Sect. 5, the isotropic compliance condition is formulated in the case of redundant manipulators, and in Sect. 6 a solution based on the minimization of the work done by the joint control torques is presented. Finally, in Sect. 7, two examples of application are presented considering a 7R and

a 9R serial manipulator, and the achievement of the desired compliance isotropy is verified by means of accurate multibody dynamics simulations.

2 Local isotropic compliance in *SE(3)*: problem formulation

According to the Denavit–Hartemberg convention, two fundamental reference frames can be defined in a serial manipulator, which are the base frame and the tool frame. With reference to Fig. 1a, the origin P of the tool frame, $R_n \equiv \{P, x_n, y_n, z_n\}$, is determined by the position vector $\overrightarrow{O_0P}$, where O_0 is the origin of the base frame $R_0 \equiv \{O_0, x_0, y_0, z_0\}$. To define the isotropic compliance property in *SE(3)*, a new frame with origin in P can be introduced, $R_P \equiv \{P, x, y, z\}$, with axes x, y, and z, defined by the unit vectors $\hat{\boldsymbol{i}}$, $\hat{\boldsymbol{j}}$, and $\hat{\boldsymbol{k}}$, respectively. The definition of this frame is based on the wrench $\boldsymbol{w} = \{\phi\hat{\boldsymbol{j}}; \mu\hat{\boldsymbol{u}}\}$ acting on the end-effector.

In the figure, the unit vector $\hat{\boldsymbol{j}}$ corresponds to the force line of action, ϕ is the force magnitude, $\hat{\boldsymbol{u}}$ is the unit vector corresponding to the axis torque u, and μ is the torque magnitude. The unit vector $\hat{\boldsymbol{k}}$ is defined as the unit vector perpendicular to $\hat{\boldsymbol{j}}$ and belonging to the plane defined by $\hat{\boldsymbol{j}}$ and $\hat{\boldsymbol{u}}$, whose sense is the same as the component of $\hat{\boldsymbol{u}}$ perpendicular to $\hat{\boldsymbol{j}}$. It follows that $\hat{\boldsymbol{i}} = \hat{\boldsymbol{j}} \times \hat{\boldsymbol{k}}$.

The torque component $\mu\hat{\boldsymbol{u}}$ of the wrench is equal to the sum of a component parallel to the force line of action, $\lambda\phi\hat{\boldsymbol{j}}$, where λ is the wrench pitch, and a component perpendicular to such line, that is, $\phi\boldsymbol{p} \times \hat{\boldsymbol{j}} = \phi p\hat{\boldsymbol{i}} \times \hat{\boldsymbol{j}} = \phi p\hat{\boldsymbol{k}}$. We define o as the screw axis of the wrench, and O the point defined by the position vector $\boldsymbol{p} = \overrightarrow{PO}$. Also, we define π as the plane xy, and σ as the plane normal to the unit vector $\hat{\boldsymbol{u}}$.

As is well known [55], the wrench $\boldsymbol{w}$ is energetically conjugated to the twist $\boldsymbol{t} = \{\Theta_\Delta\hat{\boldsymbol{h}}; \Delta P\hat{\boldsymbol{v}}\}$, where Θ_Δ is the rotation angle of the end-effector about the unit vector $\hat{\boldsymbol{h}}$, and $\Delta P\hat{\boldsymbol{v}}$ is the end-effector displacement vector. We define h as the screw axis of the twist, $\hat{\boldsymbol{h}}$ as the unit vector of h, and χ as the plane normal $\hat{\boldsymbol{h}}$. Also, we define $\boldsymbol{r} = \overrightarrow{PH}$ the vector representing the position of h with respect to P. Therefore, $\Delta P\hat{\boldsymbol{v}} = \Theta_\Delta\nu\hat{\boldsymbol{h}} + \Theta_\Delta\boldsymbol{r} \times \hat{\boldsymbol{h}}$, where ν twist pitch.

Generally, there are no particular relations between the directions of the unit vectors $\hat{\boldsymbol{j}}$ and $\hat{\boldsymbol{v}}$, which represent the directions of the applied force and of the displacement, respectively, nor between the unit vectors $\hat{\boldsymbol{u}}$ and $\hat{\boldsymbol{h}}$, the unit vectors corresponding to the axis torque and to the screw axis of the twist, respectively [16]. This case is represented in Fig. 1a. The conditions of parallelism between the unit vectors $\hat{\boldsymbol{j}}$ and $\hat{\boldsymbol{v}}$, and between the unit vectors $\hat{\boldsymbol{u}}$ and $\hat{\boldsymbol{h}}$ correspond to the *local isotropic compliance* in *SE(3)*, and it is represented in Fig. 1b.

A practical application of the *isotropic compliance* condition is depicted in Fig. 2, where a manipulator end-effector is grasping a cylindrical object in a structured workspace delimited by the plane π and, in quasi-static conditions, the interaction load is represented by the wrench $\boldsymbol{w} = \{\phi\hat{\boldsymbol{j}}; \mu\hat{\boldsymbol{u}}\}$. During its task, the end-effector must avoid collisions between the carried object and the planar boundary.

If the isotropic compliance condition not verified, as depicted in Fig. 2a, the generalized displacement is composed of a translation $\Delta P\hat{\boldsymbol{v}}$ and of a rotation $\Theta_\Delta\hat{\boldsymbol{h}}$. Since there is no control over the end-effector, the handled object could collide with the surface π.

If the local isotropic compliance condition is verified in $SE(3)$, as showed in Fig. 2b, the translation $\Delta P\hat{\boldsymbol{v}}$ of the end-effector is parallel to the force $\phi\hat{\boldsymbol{j}}$, and the rotation axis $\hat{\boldsymbol{h}}$ is parallel to the torque axis $\hat{\boldsymbol{k}}$, avoiding risk of collision to the workspace boundary.

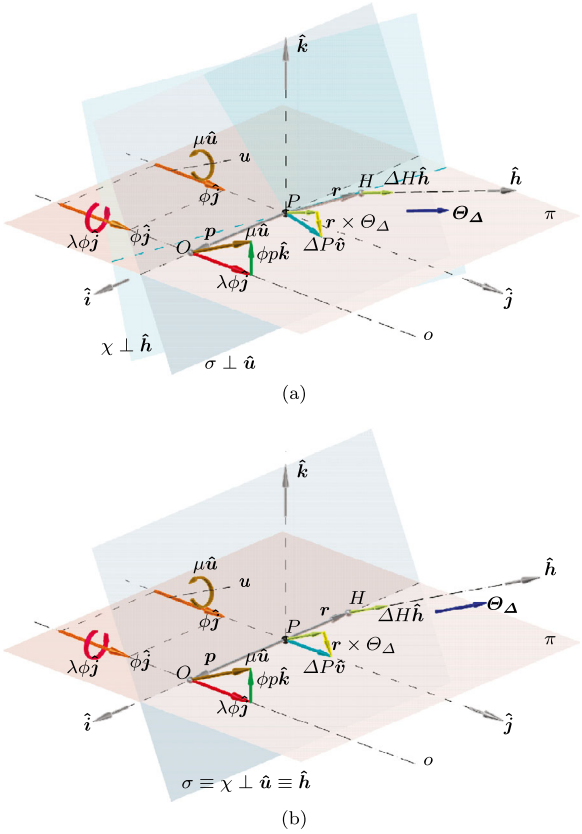

Fig. 1 (**a**) General case and (**b**) local isotropic compliance condition

3 Kinematics of redundant manipulation

The relation between the task-space velocity vector, $\dot{\boldsymbol{s}} \in \mathbb{R}^{r\times 1}$, and the joint velocity vector, $\dot{\boldsymbol{q}} \in \mathbb{R}^{n\times 1}$, can be written as

$$\dot{\boldsymbol{s}} = \mathbf{J}\dot{\boldsymbol{q}}, \tag{1}$$

where $\mathbf{J} \in \mathbb{R}^{r\times n}$ is the manipulator's Jacobian matrix. In case of redundant manipulators ($r < n$), a general solution of Eq. (1) is given by

$$\dot{\boldsymbol{q}} = \mathbf{J}^{+}\dot{\boldsymbol{s}} + \mathbf{N}\dot{\boldsymbol{q}}_0, \tag{2}$$

where $\mathbf{J}^{+} \in \mathbb{R}^{n\times r}$ is a generalized inverse of $\mathbf{J}$, $\dot{\boldsymbol{q}}_0 \in \mathbb{R}^{n\times 1}$ is an arbitrary joint velocity vector, and $\mathbf{N} \in \mathbb{R}^{n\times n}$ is a projection operator which projects $\dot{\boldsymbol{q}}_0$ into the nullspace of $\mathbf{J}$, i.e. $\mathbf{JN} \equiv \mathbf{0}$.

The first term of Eq. (2), $\dot{\boldsymbol{q}}^{*} = \mathbf{J}^{+}\dot{\boldsymbol{s}}$, defines the joint velocities necessary to obtain the given task-space velocity and represents a particular solution of Eq. (1). The second term, $\dot{\boldsymbol{q}}^{N} = \mathbf{N}\dot{\boldsymbol{q}}_0$, does not contribute to the task-space velocity, but only to the motion in the nullspace, that is, the self-motion of the redundant manipulator.

The matrices $\mathbf{J}^{+}$, $\mathbf{N}$ and the vector $\dot{\boldsymbol{q}}_0$ are not uniquely defined. A common approach to solving the redundancy problem consists in choosing a suitable symmetric positive-definite

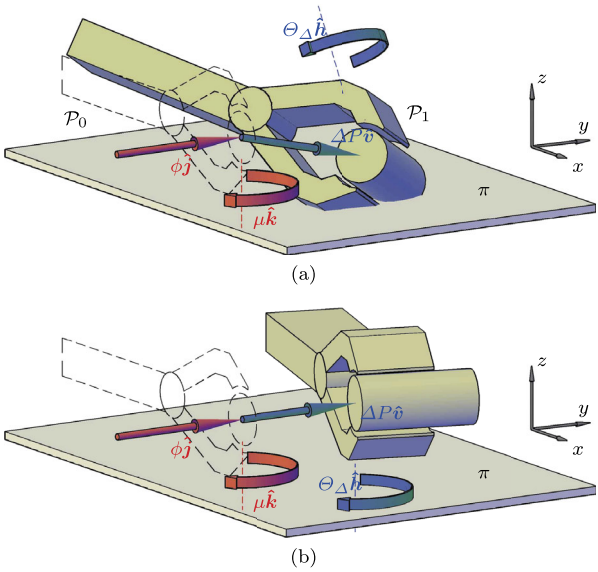

Fig. 2 End-effector handling a tool in a structured workspace: (**a**) general case and (**b**) local isotropic compliance condition in $SE(3)$

weighting matrix, $\mathbf{W} \in \mathbb{R}^{n \times n}$, in order to define the weighted right pseudoinverse of $\mathbf{J}$ as

$$\mathbf{J}^+ = \mathbf{W}^{-1}\mathbf{J}^T\left(\mathbf{J}\mathbf{W}^{-1}\mathbf{J}^T\right)^{-1}. \tag{3}$$

Considering the self-motions, the matrix

$$\mathbf{N} = \mathbf{I} - \mathbf{J}^+\mathbf{J}, \tag{4}$$

can be assumed as the nullspace projector, whereas the arbitrary joint velocity vector $\dot{\boldsymbol{q}}_0$ is usually determined by optimizing an objective function $w(\boldsymbol{q})$ of the joint variables, as [45]

$$\dot{\boldsymbol{q}}_0 = \left(\frac{\partial w(\boldsymbol{q})}{\partial \boldsymbol{q}}\right)^T. \tag{5}$$

4 Solution of the redundancy problem

In this investigation, it is assumed that the Jacobian matrix is of full (row) rank r. Since we are dealing with an essentially static problem, the relations between the task-space velocity and the joint velocity vectors can be reformulated in terms of *small* end-effector displacements and rotations, $\Delta \boldsymbol{s}$, and *small* perturbations of the configuration vector, $\Delta \boldsymbol{q}$, as

$$\Delta \boldsymbol{s} = \mathbf{J}\Delta \boldsymbol{q}, \tag{6}$$

where

$$\Delta \boldsymbol{s} = \begin{bmatrix} \mathbf{0} & \mathbf{I} \\ \mathbf{I} & \mathbf{0} \end{bmatrix}, \qquad \boldsymbol{t} = \begin{bmatrix} \Delta P \hat{\boldsymbol{v}} \\ \Theta_\Delta \hat{\boldsymbol{h}} \end{bmatrix} \tag{7}$$

and

$$\Delta \boldsymbol{q} = \mathbf{J}^+ \Delta \boldsymbol{s} + \mathbf{N}\Delta \boldsymbol{q}_0 \tag{8}$$

is a general solution of Eq. (6).

To address redundancy, the perturbation vector

$$\Delta \boldsymbol{q} = \mathbf{Q}_1 \Delta \boldsymbol{\sigma} + \mathbf{Q}_2 \Delta \boldsymbol{\alpha} \tag{9}$$

considered as a particular solution of Eq. (6). Firstly, matrices $\mathbf{Q}_1$ and $\mathbf{Q}_2$ are introduced. Then, the role of vectors $\Delta\boldsymbol{\sigma} \in \mathbb{R}^{r\times 1}$ and $\Delta\boldsymbol{\alpha} \in \mathbb{R}^{(n-r)\times 1}$ is explained.

The matrices $\mathbf{Q}_1 \in \mathbb{R}^{n\times r}$ and $\mathbf{Q}_2 \in \mathbb{R}^{n\times(n-r)}$ result from the QR decomposition of $\mathbf{J}^T \in \mathbb{R}^{n\times r}$ [56], that is,

$$\mathbf{J}^T = \mathbf{Q}\mathbf{R} = \begin{bmatrix}\mathbf{Q}_1 & \mathbf{Q}_2\end{bmatrix}\begin{bmatrix}\mathbf{R}_1 \\ \mathbf{0}\end{bmatrix} = \mathbf{Q}_1\mathbf{R}_1, \tag{10}$$

where $\mathbf{Q} \in \mathbb{R}^{n\times n}$ is an orthogonal matrix, $\mathbf{R}_1 \in \mathbb{R}^{r\times r}$ is an upper triangular matrix, and $\mathbf{0} \in \mathbb{R}^{(n-r)\times r}$ is the zero matrix.

By assuming $\mathbf{W} = \mathbf{I}$ in Eq. (3), the right pseudoinverse can be chosen as an inverse of the Jacobian matrix, that is,

$$\mathbf{J}^+ = \mathbf{J}^T\left(\mathbf{J}\mathbf{J}^T\right)^{-1}. \tag{11}$$

By making use of Eq. (10), the Jacobian matrix and its pseudoinverse become

$$\mathbf{J} = \mathbf{R}_1^T\mathbf{Q}_1^T \tag{12}$$

and

$$\mathbf{J}^+ = \mathbf{Q}_1\mathbf{R}_1^{-T}, \tag{13}$$

respectively.

Alternatively, for $\mathbf{W} \neq \mathbf{I}$, one obtains

$$\mathbf{J}^+ = \mathbf{W}^{-1}\mathbf{Q}_1\left(\mathbf{Q}_1^T\mathbf{W}^{-1}\mathbf{Q}_1\right)^{-1}\mathbf{R}_1^{-T} \tag{14}$$

Focusing on Eq. (9), it can be rewritten as

$$\Delta \boldsymbol{q} = \Delta \boldsymbol{q}^* + \Delta \boldsymbol{q}^N, \tag{15}$$

where

$$\Delta \boldsymbol{q}^* = \mathbf{Q}_1 \Delta \boldsymbol{\sigma} \tag{16}$$

defines the perturbations of the configuration vector necessary to obtain the given task-space displacement, and

$$\Delta \boldsymbol{q}^N = \mathbf{Q}_2 \Delta \boldsymbol{\alpha} \tag{17}$$

defines displacements that take place in the nullspace of the Jacobian matrix and do not contribute to the task-space displacement. In fact, the columns of $\mathbf{Q}_1$ form an orthonormal base for the range of $\mathbf{J}^T$,

$$\mathcal{R}(\mathbf{Q}_1) = \mathcal{R}\left(\mathbf{J}^T\right), \tag{18}$$

whereas the columns of $\mathbf{Q}_2$ form an orthonormal base for its orthogonal complement, that is, the nullspace of $\mathbf{J}$,

$$\mathcal{R}(\mathbf{Q}_2) = \mathcal{R}\left(\mathbf{J}^T\right)^{\perp} = \mathcal{N}(\mathbf{J}). \tag{19}$$

The role of the orthonormal bases associated with matrices $\mathbf{Q}_1$ and $\mathbf{Q}_2$ can be exemplified by considering the linear mapping between $\Delta\boldsymbol{q}$ and $\Delta\boldsymbol{s}$. By pre-multiplying both sides of Eq. (9) by $\mathbf{J}$, it follows that

$$\mathbf{J}\Delta\boldsymbol{q} = \mathbf{J}\mathbf{Q}_1^T\Delta\boldsymbol{\sigma} + \mathbf{J}\mathbf{Q}_2\Delta\boldsymbol{\alpha}. \tag{20}$$

Then, by making use of Eq. (12), Eq. (20) becomes

$$\mathbf{R}_1^T\mathbf{Q}_1^T\Delta\boldsymbol{q} = \mathbf{R}_1^T\mathbf{Q}_1^T(\mathbf{Q}_1\Delta\boldsymbol{\sigma} + \mathbf{Q}_2\Delta\boldsymbol{\alpha}) = \mathbf{R}_1^T\Delta\boldsymbol{\sigma} \tag{21}$$

and, simplifying,

$$\Delta\boldsymbol{s} = \mathbf{R}_1^T\Delta\boldsymbol{\sigma}. \tag{22}$$

It is clear that only $\Delta\boldsymbol{\sigma}$, associated with $\mathbf{Q}_1$ and $\Delta\boldsymbol{q}^*$, contributes to $\Delta\boldsymbol{s}$, whereas $\Delta\boldsymbol{\alpha}$, associated with $\mathbf{Q}_2$ and $\Delta\boldsymbol{q}^N$, does not affect the end-effector pose in the task space.

The vector $\Delta\boldsymbol{\sigma} \in \mathbb{R}^{r\times 1}$ can be obtained from Eq. (22) as

$$\Delta\boldsymbol{\sigma} = \mathbf{R}_1^{-T}\Delta\boldsymbol{s}. \tag{23}$$

The vector $\Delta\boldsymbol{\alpha} \in \mathbb{R}^{(n-r)\times 1}$, associated with the nullspace, can be determined by optimizing an arbitrarily chosen objective function of the joint coordinates perturbations, $w(\Delta\boldsymbol{q})$, by analogy with the determination of the joint velocity vector $\dot{\boldsymbol{q}}_0$ obtained by means of Eq. (5).

5 Local isotropic compliance

In order to obtain the desired isotropic compliance, suitable joint torques need to be added to the intrinsic compliance of the manipulator. In the present discussion, the case of parallel compliance is considered, i.e. the motor torques are acting in parallel with the passive compliance of the joints.

Let $\Delta\boldsymbol{s}$ be a perturbation of the configuration—displacement and rotation—in the end-effector space. Let $\Delta\boldsymbol{w}$ be a corresponding perturbation of force and moment. They are related by $\mathbf{K} \in \mathbb{R}^{r\times r}$, the stiffness matrix in the end-effector space,

$$\Delta\boldsymbol{w} = \mathbf{K}\Delta\boldsymbol{s}. \tag{24}$$

The inverse relationship makes use of the compliance matrix $\mathbf{C} = \mathbf{K}^{-1}$,

$$\Delta\boldsymbol{s} = \mathbf{C}\Delta\boldsymbol{w}. \tag{25}$$

Let $\Delta\boldsymbol{q}$ be a perturbation of the joint coordinates. The corresponding perturbation of joint torques $\Delta\boldsymbol{\tau} \in \mathbb{R}^{n\times 1}$ can be determined considering the joint stiffness matrix, $\mathbf{k} \in \mathbb{R}^{n\times n}$, by means of the relation

$$\Delta\boldsymbol{\tau} = \mathbf{k}\Delta\boldsymbol{q}. \tag{26}$$

The inverse relationship makes use of the joint compliance matrix $\mathbf{c} = \mathbf{k}^{-1}$,

$$\Delta\boldsymbol{q} = \mathbf{c}\Delta\boldsymbol{\tau}. \tag{27}$$

The perturbation of the end-effector configuration is related to the perturbation of the joint coordinates by the Jacobian matrix $\mathbf{J}$,

$$\Delta \boldsymbol{s} = \mathbf{J}\Delta \boldsymbol{q}. \tag{28}$$

The equivalence between the work done by a perturbation of joint torques and of end-effector force and moment for the corresponding joint and end-effector motion perturbation $\Delta \boldsymbol{q}^T \Delta \boldsymbol{\tau} = \Delta \boldsymbol{s}^T \Delta \boldsymbol{w} = \Delta \boldsymbol{q}^T \mathbf{J}^T \Delta \boldsymbol{w}$ yields the relationship between end-effector loads and joint torques

$$\Delta \boldsymbol{\tau} = \mathbf{J}^T \Delta \boldsymbol{w}. \tag{29}$$

Expressing the end-effector force and moment and the joint torques as functions of the corresponding configuration perturbations through the previously introduced constitutive relationships, $\Delta \boldsymbol{q}^T \mathbf{k} \Delta \boldsymbol{q} = \Delta \boldsymbol{s}^T \mathbf{K} \Delta \boldsymbol{s} = \Delta \boldsymbol{q}^T \mathbf{J}^T \mathbf{K} \mathbf{J} \Delta \boldsymbol{q}$ yields the relationship between the stiffness matrix in the end-effector space and the corresponding joint stiffness matrix,

$$\mathbf{k} = \mathbf{J}^T \mathbf{K} \mathbf{J}. \tag{30}$$

Similarly, considering the inverse of the constitutive relationships, $\Delta \boldsymbol{w}^T \mathbf{C} \Delta \boldsymbol{w} = \Delta \boldsymbol{\tau}^T \mathbf{c} \Delta \boldsymbol{\tau} = \Delta \boldsymbol{w}^T \mathbf{J} \mathbf{c} \mathbf{J}^T \Delta \boldsymbol{w}$ one obtains the relationship between the joint compliance and the end-effector compliance matrix,

$$\mathbf{C} = \mathbf{J} \mathbf{c} \mathbf{J}^T, \tag{31}$$

whose inverse yields a direct relationship between the joint stiffness matrix and the corresponding end-effector stiffness matrix,

$$\mathbf{K} = \left(\mathbf{J} \mathbf{k}^{-1} \mathbf{J}^T \right)^{-1} \tag{32}$$

Isotropic compliance is obtained by adding a control stiffness, i.e. the "active" stiffness that is needed to obtain the desired end-effector stiffness $\mathbf{K}$, by means of the joint motors. The control stiffness

$$\mathbf{k}_c = -\mathbf{k}_p + \mathbf{J}^T \mathbf{K} \mathbf{J} \tag{33}$$

replaces the passive stiffness $\mathbf{k}_p$ with a matrix that provides the desired end-effector stiffness, such that $\mathbf{k} = \mathbf{k}_p + \mathbf{k}_c = \mathbf{J}^T \mathbf{K} \mathbf{J}$.

In case of manipulator redundancy, the control stiffness is not uniquely defined. In general, it can be formulated as

$$\mathbf{k}_c = -\mathbf{k}_p + \mathbf{J}^T \mathbf{K} \mathbf{J} + \mathbf{Q}_2^T \boldsymbol{\gamma} \mathbf{Q}_2, \tag{34}$$

where the symmetric matrix $\boldsymbol{\gamma}$ does not affect the stiffness in the end-effector space. It represents the degree of arbitrariness provided by the redundancy, which can be determined by minimizing some cost function.

Theorem 1 *$\boldsymbol{\gamma} \in Sym(n-r)$ does not affect the Cartesian stiffness matrix.*

Proof The joint stiffness matrix, $\mathbf{k} = \mathbf{k}_p + \mathbf{k}_c$, is expressed in the rangespace and nullspace of the joint Jacobian matrix,

$$\mathbf{Q}^T \mathbf{k} \mathbf{Q} = \begin{bmatrix} \mathbf{R}_1 \mathbf{K} \mathbf{R}_1^T & \mathbf{0} \\ \mathbf{0} & \boldsymbol{\gamma} \end{bmatrix} \tag{35}$$

It is worth noticing that the choice of $\boldsymbol{\gamma}$ affects the definiteness of the matrix in Eq. (35) with respect to coordinates that express the solution in the nullspace of $\mathbf{J}$, $\mathbf{Q}_2$. For example, $\boldsymbol{\gamma} = \mathbf{0}$ would make matrix $\mathbf{k}$ singular with respect to joint displacement perturbations in the nullspace of $\mathbf{J}$, whereas a non-definite matrix would make the reference solution unstable. To overcome such problems, $\boldsymbol{\gamma} > 0$ is required.

From Eq. (35), the inverse of the reoriented joint stiffness matrix can be determined as

$$\mathbf{k}^{-1} = \mathbf{Q} \begin{bmatrix} \mathbf{R}_1^{-T} \mathbf{K}^{-1} \mathbf{R}_1^{-1} & \mathbf{0} \\ \mathbf{0} & \boldsymbol{\gamma}^{-1} \end{bmatrix} \mathbf{Q}^T \tag{36}$$

and used to compute the tool space compliance matrix, $\mathbf{C}$.

In fact, the compliance matrix in the joint space is mapped into the Cartesian space by means of the Jacobian as

$$\mathbf{C} = \mathbf{J} \mathbf{c} \mathbf{J}^T, \tag{37}$$

where $\mathbf{c} = \mathbf{k}^{-1}$. Therefore, by substituting Eq. (36) in Eq. (37), and by making use of Eq. (12), it follows that

$$\mathbf{C} = \mathbf{R}_1^T \mathbf{Q}_1^T \mathbf{Q} \begin{bmatrix} \mathbf{R}_1^{-T} \mathbf{K}^{-1} \mathbf{R}_1^{-1} & \mathbf{0} \\ \mathbf{0} & \boldsymbol{\gamma}^{-1} \end{bmatrix} \mathbf{Q}^T \mathbf{Q}_1 \mathbf{R}_1,$$

where $\mathbf{C} = \mathbf{K}^{-1}$. □

6 Redundancy exploitation

The redundancy is exploited by choosing matrix $\boldsymbol{\gamma}$ such that some cost function is minimized. Although several cost functions can be envisaged, in the following the work done by control torques in vector $\Delta \boldsymbol{\tau}_c$ for the corresponding joint motion is considered, namely $\min(\Delta \boldsymbol{q}^T \Delta \boldsymbol{\tau}_c)^2$. Since the problem results in a positive-definite quadratic cost function, an analytical solution can be obtained through a Lyapunov algebraic matrix equation.

The control torque perturbations vector is required, which is defined as

$$\Delta \boldsymbol{\tau}_c = \mathbf{k}_c \Delta \boldsymbol{q} = \left(-\mathbf{k}_p + \mathbf{J}^T \mathbf{K} \mathbf{J} + \mathbf{Q}_2 \boldsymbol{\gamma} \mathbf{Q}_2^T \right) \Delta \boldsymbol{q}. \tag{38}$$

Considering the coordinate transformation $\Delta \boldsymbol{q} = \mathbf{Q}_1 \Delta \boldsymbol{\sigma} + \mathbf{Q}_2 \Delta \boldsymbol{\alpha}$ of Eq. (9), the work, possibly with some weight $\mathbf{W}$ on each joint's contribution, is

$$\begin{aligned} \mathcal{L} &= \Delta \boldsymbol{q}^T \mathbf{W} \Delta \boldsymbol{\tau}_c \\ &= \begin{Bmatrix} \boldsymbol{\sigma} \\ \boldsymbol{\alpha} \end{Bmatrix}^T \begin{bmatrix} \mathbf{Q}_1^T \mathbf{W} \left(\mathbf{J}^T \mathbf{K} \mathbf{R}_1^T - \mathbf{k}_p \mathbf{Q}_1 \right) & \mathbf{Q}_1^T \mathbf{W} \left(\mathbf{Q}_2 \boldsymbol{\gamma} - \mathbf{k}_p \mathbf{Q}_2 \right) \\ \mathbf{Q}_2^T \mathbf{W} \left(\mathbf{J}^T \mathbf{K} \mathbf{R}_1^T - \mathbf{k}_p \mathbf{Q}_1 \right) & \mathbf{Q}_2^T \mathbf{W} \left(\mathbf{Q}_2 \boldsymbol{\gamma} - \mathbf{k}_p \mathbf{Q}_2 \right) \end{bmatrix} \begin{Bmatrix} \boldsymbol{\sigma} \\ \boldsymbol{\alpha} \end{Bmatrix} \\ &= \begin{Bmatrix} \boldsymbol{\sigma} \\ \boldsymbol{\alpha} \end{Bmatrix}^T \begin{bmatrix} \mathbf{M}_{11} & \mathbf{M}_{12} \\ \mathbf{M}_{21} & \mathbf{M}_{22} \end{bmatrix} \begin{Bmatrix} \boldsymbol{\sigma} \\ \boldsymbol{\alpha} \end{Bmatrix}, \end{aligned} \tag{39}$$

with straightforward definition of the block-elements $\mathbf{M}_{ij}$, $i, j = 1, 2$, of matrix $\mathbf{M}$, thus, noticing that only $\mathbf{M}_{12}$ and $\mathbf{M}_{22}$ depend on $\boldsymbol{\gamma}$,

$$
\begin{aligned}
(\mathcal{L})^2 &= \mathcal{L}^T \mathcal{L} \\
&= \mathrm{tr}\left(\begin{Bmatrix} \boldsymbol{\sigma} \\ \boldsymbol{\alpha} \end{Bmatrix}^T \begin{bmatrix} \mathbf{M}_{11}^T & \mathbf{M}_{21}^T \\ \mathbf{M}_{12}^T & \mathbf{M}_{22}^T \end{bmatrix} \begin{Bmatrix} \boldsymbol{\sigma} \\ \boldsymbol{\alpha} \end{Bmatrix} \begin{Bmatrix} \boldsymbol{\sigma} \\ \boldsymbol{\alpha} \end{Bmatrix}^T \begin{bmatrix} \mathbf{M}_{11} & \mathbf{M}_{12} \\ \mathbf{M}_{21} & \mathbf{M}_{22} \end{bmatrix} \begin{Bmatrix} \boldsymbol{\sigma} \\ \boldsymbol{\alpha} \end{Bmatrix} \right) \\
&= \mathrm{tr}\left(\begin{Bmatrix} \boldsymbol{\sigma} \\ \boldsymbol{\alpha} \end{Bmatrix} \begin{Bmatrix} \boldsymbol{\sigma} \\ \boldsymbol{\alpha} \end{Bmatrix}^T \begin{bmatrix} \mathbf{M}_{11}^T & \mathbf{M}_{21}^T \\ \mathbf{M}_{12}^T & \mathbf{M}_{22}^T \end{bmatrix} \begin{Bmatrix} \boldsymbol{\sigma} \\ \boldsymbol{\alpha} \end{Bmatrix} \begin{Bmatrix} \boldsymbol{\sigma} \\ \boldsymbol{\alpha} \end{Bmatrix}^T \begin{bmatrix} \mathbf{M}_{11} & \mathbf{M}_{12} \\ \mathbf{M}_{21} & \mathbf{M}_{22} \end{bmatrix} \right) \\
&= \mathrm{tr}\left(\begin{bmatrix} \mathbf{H}_{11} & \mathbf{H}_{12} \\ \mathbf{H}_{12}^T & \mathbf{H}_{22} \end{bmatrix} \begin{bmatrix} \mathbf{M}_{11}^T & \mathbf{M}_{21}^T \\ \mathbf{M}_{12}^T & \mathbf{M}_{22}^T \end{bmatrix} \begin{bmatrix} \mathbf{H}_{11} & \mathbf{H}_{12} \\ \mathbf{H}_{12}^T & \mathbf{H}_{22} \end{bmatrix} \begin{bmatrix} \mathbf{M}_{11} & \mathbf{M}_{12} \\ \mathbf{M}_{21} & \mathbf{M}_{22} \end{bmatrix} \right) \\
&= \mathrm{tr}\begin{pmatrix} \mathbf{H}_{12}\mathbf{M}_{12}^T \left(\mathbf{H}_{11}\mathbf{M}_{11} + \mathbf{H}_{12}\mathbf{M}_{21}\right) \\ + \mathbf{H}_{12}\mathbf{M}_{22}^T \left(\mathbf{H}_{12}^T\mathbf{M}_{11} + \mathbf{H}_{22}\mathbf{M}_{21}\right) \end{pmatrix} \\
&\quad + \mathrm{tr}\begin{pmatrix} \left(\mathbf{H}_{12}^T\mathbf{M}_{11}^T + \mathbf{H}_{22}\mathbf{M}_{12}^T\right) \left(\mathbf{H}_{11}\mathbf{M}_{12} + \mathbf{H}_{12}\mathbf{M}_{22}\right) \\ + \left(\mathbf{H}_{12}^T\mathbf{M}_{21}^T + \mathbf{H}_{22}\mathbf{M}_{22}^T\right) \left(\mathbf{H}_{12}^T\mathbf{M}_{12} + \mathbf{H}_{22}\mathbf{M}_{22}\right) \end{pmatrix} \\
&\quad + \cdots \text{ (terms that do not depend on } \boldsymbol{\gamma}\text{)},
\end{aligned} \tag{40}
$$

where the symmetric, positive-definite matrix $\mathbf{H}$, and the corresponding sub-matrices $\mathbf{H}_{11}$, $\mathbf{H}_{22}$, and $\mathbf{H}_{12}$, represent the importance associated with each of the degrees of freedom of the system, which stems from independently perturbing each of the coordinates, namely

$$
\mathbf{H} = \sum_{i=1,N} w_i \boldsymbol{e}_i \boldsymbol{e}_i^T \tag{41}
$$

with respect to base $\boldsymbol{e}_i$, weighted by $w_i > 0$. It is the identity matrix in the case of equal weight for all directions, regardless of the base, since an orthogonal coordinate transformation is used in Eq. (9).

The minimization of the cost function implies the solution of the Lyapunov equation

$$
\begin{aligned}
\mathbf{0} &= \mathbf{H}_{22}^{-1}\mathbf{Q}_2^T\mathbf{W}\mathbf{Q}\mathbf{H}\mathbf{Q}^T\mathbf{W}\mathbf{Q}_2\boldsymbol{\gamma} + \boldsymbol{\gamma}\mathbf{Q}_2^T\mathbf{W}\mathbf{Q}\mathbf{H}\mathbf{Q}^T\mathbf{W}\mathbf{Q}_2\mathbf{H}_{22}^{-1} \\
&\quad + \mathbf{H}_{22}^{-1}\mathbf{Q}_2^T\mathbf{W}\mathbf{Q}\mathbf{H}\begin{bmatrix} \mathbf{M}_{11} \\ \mathbf{M}_{21} \end{bmatrix}\mathbf{H}_{12}\mathbf{H}_{22}^{-1} \\
&\quad - \mathbf{H}_{22}^{-1}\mathbf{Q}_2^T\mathbf{W}\mathbf{Q}\mathbf{H}\mathbf{Q}^T\mathbf{W}\mathbf{k}_p\mathbf{Q}_2 - \mathbf{Q}_2^T\mathbf{k}_p\mathbf{W}\mathbf{Q}\mathbf{H}\mathbf{Q}^T\mathbf{W}\mathbf{Q}_2\mathbf{H}_{22}^{-1} \\
&\quad + \mathbf{H}_{22}^{-1}\mathbf{H}_{12}^T\begin{bmatrix} \mathbf{M}_{11}^T & \mathbf{M}_{21}^T \end{bmatrix}\mathbf{H}\mathbf{Q}^T\mathbf{W}\mathbf{Q}_2\mathbf{H}_{22}^{-1}.
\end{aligned} \tag{42}
$$

For $\mathbf{H} = \mathbf{I}$, i.e. $\mathbf{H}_{11} = \mathbf{I}$, $\mathbf{H}_{22} = \mathbf{I}$, and $\mathbf{H}_{12} = \mathbf{0}$, one obtains

$$
\mathbf{0} = \mathbf{Q}_2^T\mathbf{W}^2\mathbf{Q}_2\boldsymbol{\gamma} + \boldsymbol{\gamma}\mathbf{Q}_2^T\mathbf{W}^2\mathbf{Q}_2 - \mathbf{Q}_2^T\left(\mathbf{W}^2\mathbf{k}_p + \mathbf{k}_p\mathbf{W}^2\right)\mathbf{Q}_2 \tag{43}
$$

Furthermore, for $\mathbf{W} = \mathbf{I}$, i.e. when the actual work is minimized, the solution is

$$
\boldsymbol{\gamma} = \mathbf{Q}_2^T\mathbf{k}_p\mathbf{Q}_2, \tag{44}
$$

which yields the control stiffness matrix

$$
\mathbf{k}_c = \mathbf{J}^T\mathbf{K}\mathbf{J} + \mathbf{Q}_2\mathbf{Q}_2^T\mathbf{k}_p\mathbf{Q}_2\mathbf{Q}_2^T - \mathbf{k}_p. \tag{45}
$$

Table 1 7R manipulator: Denavit–Hartenberg parameters and joint passive stiffness coefficients

Joint	d (m)	a (m)	α (deg)	k_p (Nm/rad)
1	0	0	90	800
2	0	0.432	0	880
3	0.150	0.020	−90	710
4	0.432	0	90	730
5	0	0	−90	660
6	0	0.200	0	750
7	0.250	0.250	−90	690

From a physical point of view, the control system does not work against the passive stiffness in the nullspace of $\mathbf{J}^T$.

7 Examples of application

In this section, the local isotropic compliance property is achieved in two redundant systems with different degrees of redundancy, which are a 7R and a 9R serial manipulator, considering active and passive stiffness in parallel arrangement.

7.1 Seven-DoF manipulator

The 7R manipulator under study is depicted in Fig. 3a in its reference posture ($\boldsymbol{q} = \mathbf{0}$). Table 1 lists its Denavit–Hartenberg parameters and joint passive stiffness coefficients $k_{p_1}, \ldots, k_{p_7}$.

The perturbation load is applied to the tip of the end-effector. The property is achieved in two different postures, defined in radians by the joint coordinates vectors

$$\boldsymbol{q}_a = [0, -0.39, -0.45, -0.35, 0.45, -0.39, 0.52],$$
$$\boldsymbol{q}_b = [0, 0.10, -1.85, -1.55, 1.55, 1.85, -1.20],$$

and depicted in Figs. 3b and 3c, respectively.

7.1.1 Control-matrix computation

The control matrix can be computed according to the following algorithm. Firstly, the desired compliance response of the end-effector is defined by the assigning compliance matrix in the Cartesian space. In order to achieve the isotropic condition, $\mathbf{C}$ must be a block matrix whose diagonal blocks are scalar matrices and whose off-diagonal blocks are zero matrices, i.e.

$$\mathbf{C} = \begin{bmatrix} \tilde{c}_d \mathbf{I} & \mathbf{0} \\ \mathbf{0} & \tilde{c}_r \mathbf{I} \end{bmatrix}. \tag{46}$$

In Eq. (46), $\mathbf{I} \in \mathbb{R}^{3\times3}$ is the identity matrix, $\mathbf{0} \in \mathbb{R}^{3\times3}$ is the zero matrix, and $\tilde{c}_d$ and $\tilde{c}_r$ are the compliance coefficients associated to linear displacements and rotations, respectively. For

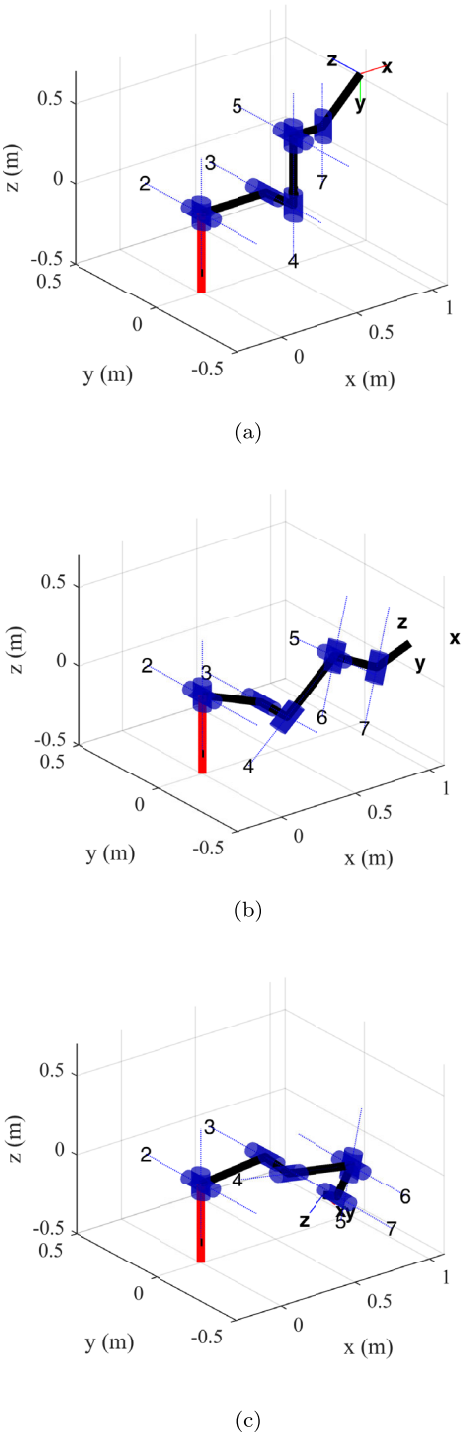

Fig. 3 Seven-DoF manipulator in: (**a**) posture defined by $\boldsymbol{q} = \boldsymbol{0}$; (**b**) posture defined by $\boldsymbol{q}_a$; (**c**) posture defined by $\boldsymbol{q}_b$

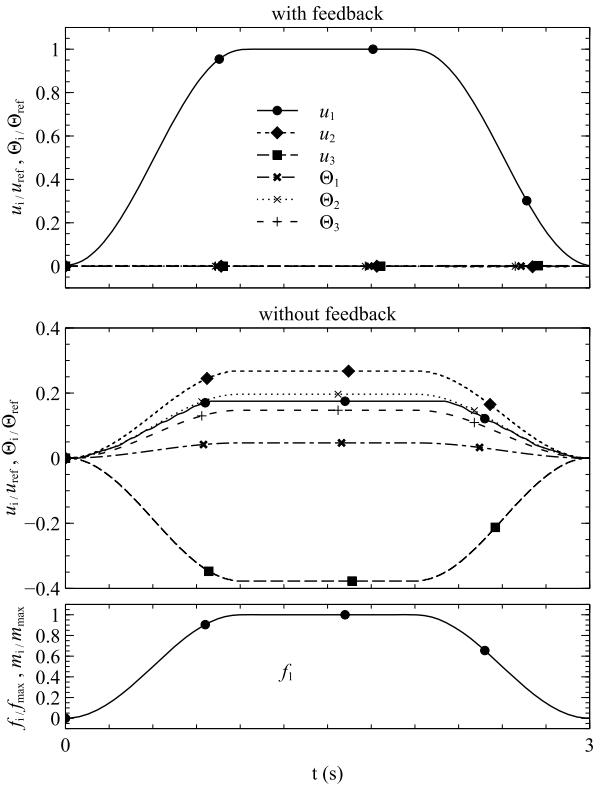

Fig. 4 Seven-DoF manipulator in the posture $\boldsymbol{q}_a$: end-effector displacements and rotations, with and without control action, for the first 3 s of simulation (force applied in the x-axis direction)

the following examples, the compliance coefficients are set as

$$\begin{aligned} \tilde{c}_d &= 2.0 \cdot 10^{-3}\ \mathrm{m\,N^{-1}}, \\ \tilde{c}_r &= 1.7 \cdot 10^{-3}\ \mathrm{N^{-1}\,m^{-1}\,rad}. \end{aligned} \tag{47}$$

Then, the stiffness matrix can be calculated as $\mathbf{K} = \mathbf{C}^{-1}$.

Considering the first posture, the Jacobian matrix corresponding to $\boldsymbol{q}_a$ is

$$\mathbf{J} = \begin{bmatrix} 0.287 & 1.209 & 0.000 & 0.000 & 0.000 & 1.000 \\ -0.197 & 0.000 & 1.208 & 0.000 & -1.000 & 0.000 \\ -0.362 & 0.000 & 0.810 & 0.000 & -1.000 & 0.000 \\ 0.092 & 0.249 & -0.102 & 0.746 & 0.000 & 0.666 \\ -0.049 & 0.141 & 0.477 & -0.228 & -0.940 & 0.255 \\ \hline 0.138 & 0.393 & -0.125 & 0.400 & 0.148 & 0.904 \\ 0.028 & 0.243 & -0.052 & 0.400 & 0.148 & 0.904 \end{bmatrix},$$

and its QR decomposition can performed as in Eq. (10), in order to obtain $\mathbf{Q}_1$, $\mathbf{Q}_2$ and $\mathbf{R}_1$. Therefore, the matrix $\boldsymbol{\gamma}$ can be determined by using Eq. (44), considering the values of $\mathbf{k}_p$

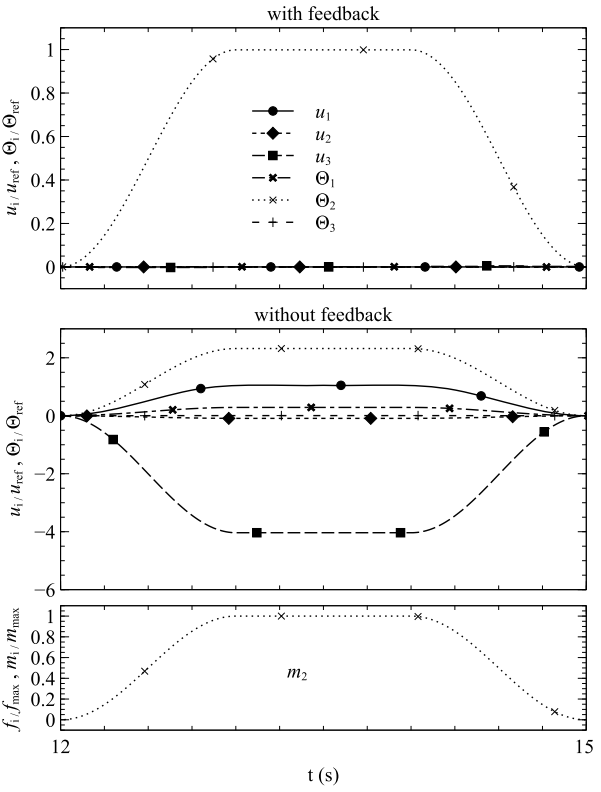

Fig. 5 Seven-DoF manipulator in the posture $\boldsymbol{q}_a$: end-effector displacements and rotations, with and without control action, for the simulation time from 12 s to 15 s (moment applied in the y-axis direction)

listed in Table 1. Finally, the control stiffness matrix, from Eq. (34), results in

$$\mathbf{k}_c = \begin{bmatrix} 5.68e2 & -2.66e1 & -6.45e1 & 5.70e2 & 2.36e2 & 7.27e2 & 7.23e2 \\ -2.66e1 & 4.58e2 & 1.11e3 & -6.81e1 & 8.47e2 & -1.89e2 & -1.13e2 \\ -6.45e1 & 1.11e3 & 2.90e2 & -7.95e1 & 7.42e2 & -6.87e1 & -1.75e2 \\ 5.70e2 & -6.81e1 & -7.95e1 & -7.67e1 & 4.80e0 & 4.84e2 & 6.34e2 \\ 2.36e2 & 8.47e2 & 7.42e2 & 4.80e0 & 6.09e1 & -6.64e1 & 4.36e1 \\ 7.27e2 & -1.89e2 & -6.87e1 & 4.84e2 & -6.64e1 & 4.05e2 & 3.34e2 \\ 7.23e2 & -1.13e2 & -1.75e2 & 6.34e2 & 4.36e1 & 3.34e2 & 1.29e2 \end{bmatrix}.$$

By following an analogous procedure, the matrices $\mathbf{J}$ and $\mathbf{k}_c$ can be evaluated for the second posture, $\boldsymbol{q}_b$, resulting in

$$\mathbf{J} = \begin{bmatrix} -0.104 & 0.937 & 0.000 & 0.000 & 0.000 & 1.000 \\ 0.413 & 0.000 & 0.937 & 0.000 & -1.000 & 0.000 \\ 0.456 & 0.000 & 0.508 & 0.000 & -1.000 & 0.000 \\ 0.045 & 0.338 & 0.250 & 0.98399 & 0.000 & -0.178 \\ -0.242 & 0.149 & 0.047 & 0.17821 & -0.021 & 0.984 \\ -0.364 & 0.010 & -0.080 & 0.024168 & 1.000 & 0.017 \\ -0.184 & 0.007 & -0.169 & 0.024168 & 1.000 & 0.017 \end{bmatrix}$$

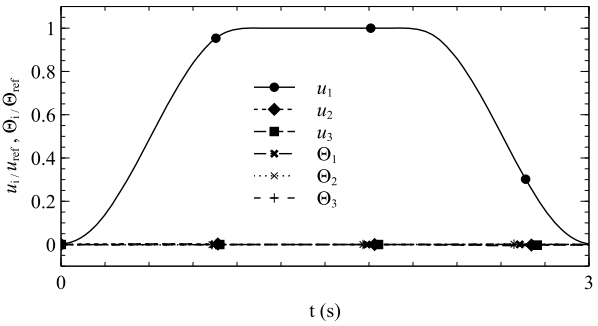

Fig. 6 Seven-DoF manipulator in the posture $\boldsymbol{q}_b$: end-effector displacements and rotations, with and without control action, for the first 3 s of simulation (force applied in the x-axis direction)

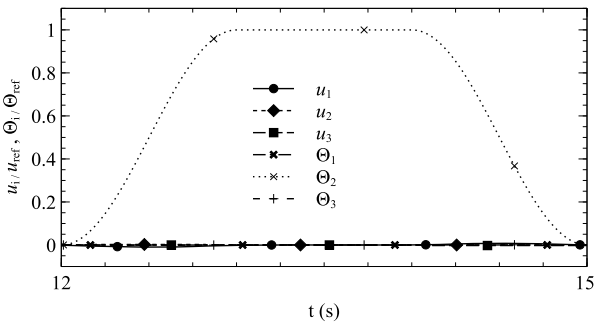

Fig. 7 Seven-DoF manipulator in the posture $\boldsymbol{q}_b$: end-effector displacements and rotations, with and without control action, for the simulation time from 12 s to 15 s (moment applied in the y-axis direction)

and

$$\mathbf{k}_c = \begin{bmatrix} 2.33e2 & -2.13e1 & -2.42e1 & 5.13e1 & 6.61e2 & 3.32e1 & 2.30e1 \\ -2.13e1 & 3.32e2 & 7.35e2 & 1.28e2 & -1.42e1 & -8.58e2 & -6.35e2 \\ -2.42e1 & 7.35e2 & 4.59e2 & 7.04e1 & -3.41e1 & -3.98e2 & -8.05e2 \\ 5.13e1 & 1.28e2 & 7.04e1 & -5.22e1 & 2.56e1 & -7.21e0 & -1.05e1 \\ 6.61e2 & -1.42e1 & -3.41e1 & 2.56e1 & -3.01e1 & 4.05e1 & 2.00e1 \\ 3.32e1 & -8.58e2 & -3.98e2 & -7.21e0 & 4.05e1 & 1.55e2 & 5.17e2 \\ 2.30e1 & -6.35e2 & -8.05e2 & -1.05e1 & 2.00e1 & 5.17e2 & -2.06e1 \end{bmatrix},$$

respectively.

7.1.2 Verification by multibody simulation

The system response has been verified by means of a dynamic simulation performed using MBDyn, a free general-purpose multibody solver developed at Politecnico di Milano [57]. The multibody model is made of seven rigid bodies and seven revolute joints. The constitutive law of each joint is characterized by the corresponding nominal torsional stiffness, k_p, as listed in Table 1, and a viscous damping term equal to $10^{-3} \cdot k_p$ Nm s/rad. Inertia properties have not been considered, since only (quasi-)static problems have been addressed.

A sequence of three independent forces and three independent moments is applied to the end-effector. Each force and moment is directed, respectively, along and about one of the coordinate axes; the magnitude of each force and moment is equal to 0.2 N and 0.5 Nm, respectively. These values have been chosen to produce a detectable configuration change, yet small enough to neglect kinematic nonlinearities in the perturbed solution. Each force

Table 2 9R manipulator: Denavit–Hartenberg parameters and joint passive stiffness coefficients

Joint	d (m)	a (m)	α (deg)	k_p (Nm/rad)
1	0.200	0	90	800
2	0	0	−90	880
3	0.200	0	90	710
4	0	0	−90	730
5	0.200	0	90	660
6	0	0	−90	750
7	0.200	0	90	690
8	0	0	−90	640
9	0.100	0	0	730

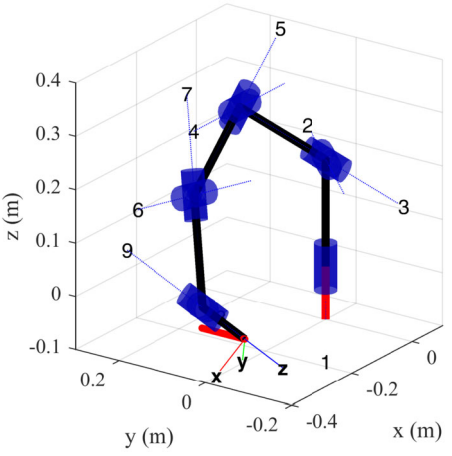

Fig. 8 Nine-DoF serial manipulator: initial posture and prescribed end-effector trajectory parallel to the y-axis (red line)

and moment is slowly increased following a regular pattern (a sequence of $(1 - \cos(t))$-shaped trajectories), then kept constant for some time, and subsequently slowly brought back to zero. The small applied loads induce correspondingly small changes of configuration; thus, the feedback gain matrix can be held constant.

The results presented in Fig. 4 refer to the first posture, $\boldsymbol{q}_a$, defined in Sect. 7.1.1. The figure shows the applied loads and the corresponding end-effector displacements and rotations, $\boldsymbol{u}$ and $\boldsymbol{\Theta}$, computed with and without the control action. The first 3 seconds of simulation refer to the loading cycle along the x axis. It is clear that when the feedback action is present, the solution provides almost perfectly the sought local isotropic compliance. Figure 5 shows the range between 15 s and 18 s of the simulation, which refer to the moment loading along the y axis. The responses obtained when the end-effector is loaded with a force or a moment in the other directions are qualitatively identical, and reported in the appendix. It is worth noting that, during the loading and unloading phases, the end-effector presents some negligible deviations (three orders of magnitudes) from the isotropic compliance behavior because of unavoidable viscous friction terms.

As a further verification of the proposed approach, Figs. 6 and 7 report, under the same loads, the end-effector displacement and finite rotations vectors obtained, with feedback, with the second posture, $\boldsymbol{q}_b$, defined in Sect. 7.1.1. Further results are reported in Appendix.

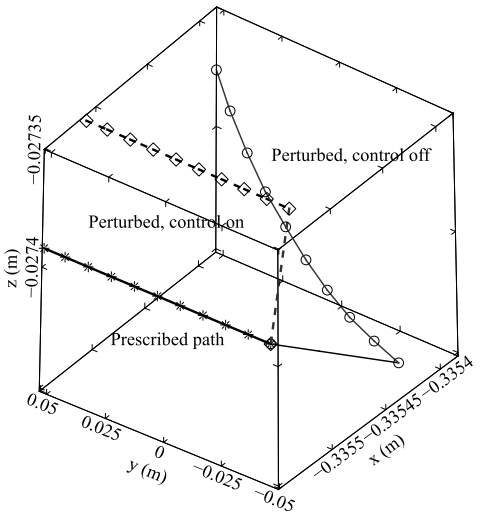

Fig. 9 Nine-DoF manipulator end-effector paths: no perturbation forces at the tip (asterisk), perturbation forces at the tip with no feedback control (circle), and perturbation forces at the tip with feedback control (square)

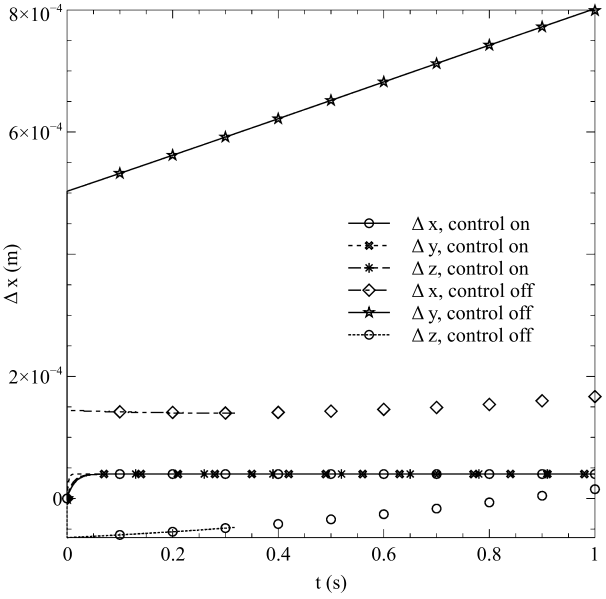

Fig. 10 Nine-DoF manipulator: end-effector displacements with respect to the prescribed path

7.2 Nine-DoF manipulator

In this subsection, a more complex case is examined. In fact, a higher degree of redundancy is introduced and, instead of an assigned posture, an assigned task is considered. Table 2 lists the Denavit–Hartenberg parameters and the joint passive stiffness coefficients of a 9R serial manipulator.

The assigned task consists of the generation of a straight path for the end-effector, keeping it in a constant orientation. More specifically, starting from the posture defined by the

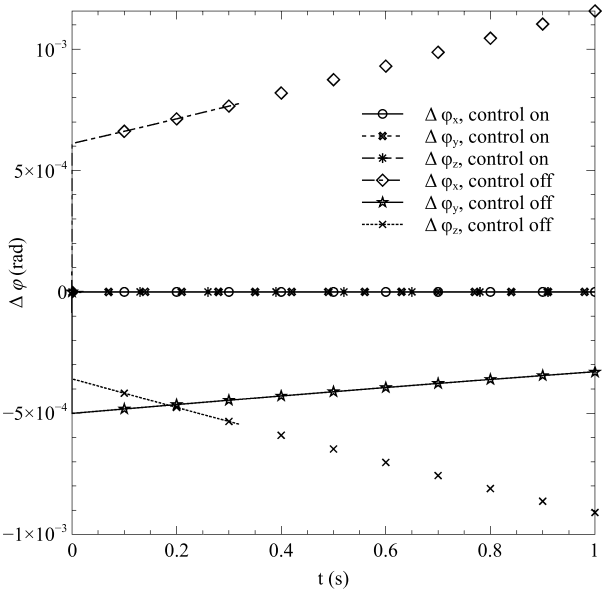

Fig. 11 Nine-DoF manipulator: end-effector rotations with respect to the prescribed path

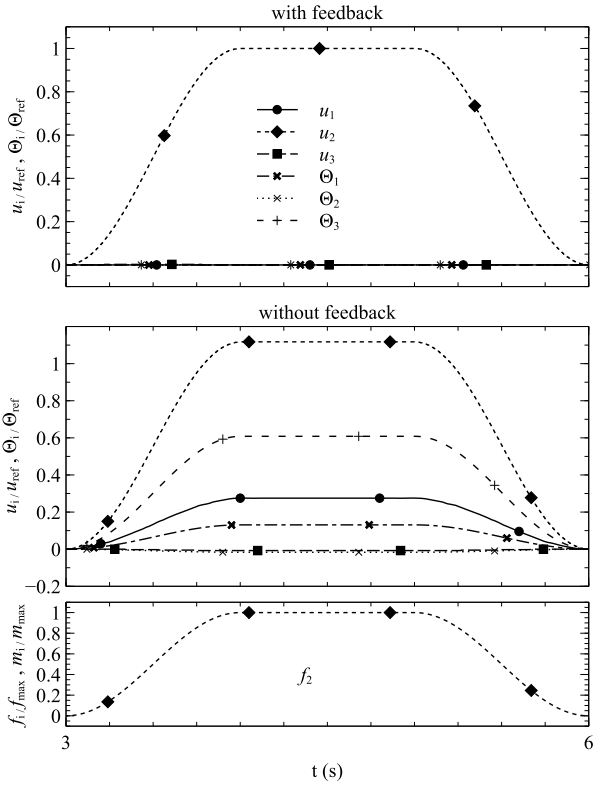

Fig. 12 Seven-DoF manipulator in the posture $\boldsymbol{q}_a$: end-effector displacements and rotations, with and without control action, for the simulation time from 3 s to 6 s (force applied in the y-axis direction)

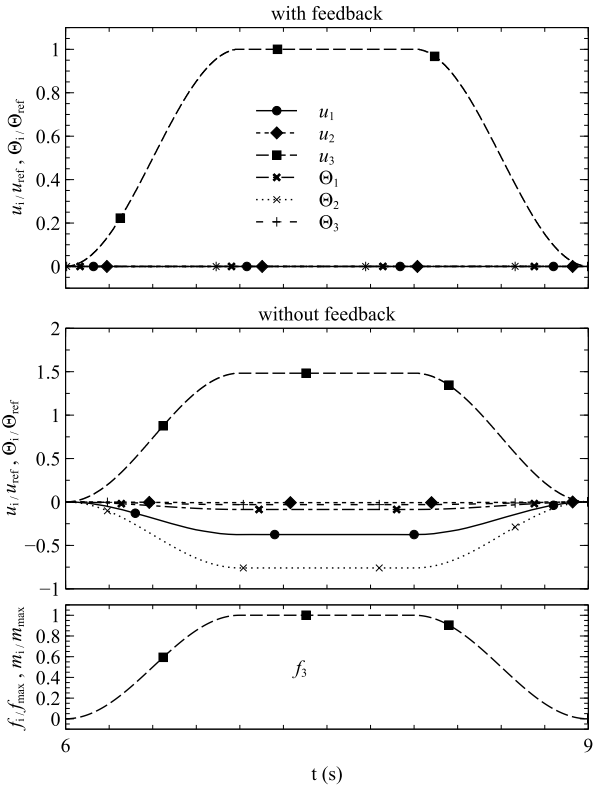

Fig. 13 Seven-DoF manipulator in the posture $\boldsymbol{q}_a$: end-effector displacements and rotations, with and without control action, for the simulation time from 6 s to 9 s (force applied in the z-axis direction)

joint coordinates vector

$$\boldsymbol{q} = [-0.77, 0.98, 0.66, 1.42, -0.16, 0.66, 0.83, 0.87, -0.40],$$

a line segment parallel to the y-axis and with length equal to 10 cm is considered. Both the manipulator in the initial posture and the prescribed path are depicted in Fig. 8. The line segment is defined by 100 equally spaced points, and for each point the corresponding joint coordinates values are calculated. Any intermediate reference posture during the simulation is computed by linearly interpolating, as a function of time, the joint coordinates. To verify the effectiveness of the proposed control approach, the control stiffness matrix $\mathbf{k}_c$ is also computed at each point, and linearly interpolated for any intermediate posture. The compliance coefficients are set as

$$\begin{aligned} \tilde{c}_d &= 2.0 \cdot 10^{-5}\ \text{mN}^{-1}, \\ \tilde{c}_r &= 1.7 \cdot 10^{-5}\ \text{N}^{-1}\ \text{m}^{-1}\ \text{rad}. \end{aligned} \tag{48}$$

During a simulation time of 1 s, a constant disturbance force, $\boldsymbol{f} = [2, 2, 2]$ N, is applied to the end-effector. Figure 9 compares the end-effector paths in three different cases: (a) no perturbation forces at the tip, (b) perturbation forces at the tip with no feedback control, (c) perturbation forces at the tip with feedback control. As it can be seen from the figure, in the case of active stiffness regulation the end-effector path is parallel to the prescribed one, with a constant displacement equal to $\boldsymbol{s} = [4, 4, 4] \cdot 10^{-5}$ m.

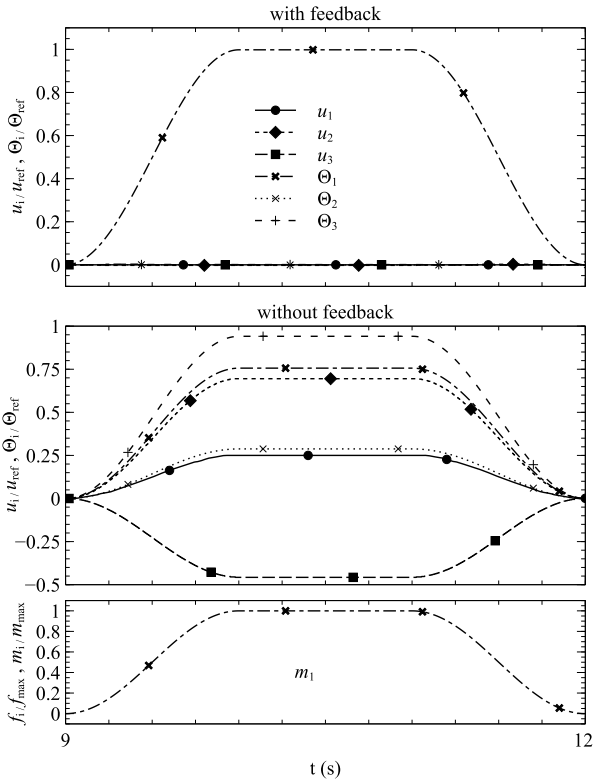

Fig. 14 Seven-DoF manipulator in the posture $\boldsymbol{q}_a$: end-effector displacements and rotations, with and without control action, for the simulation time from 9 s to 12 s (moment applied in the x-axis direction)

Figure 10 compares the end-effector displacements due to the perturbation forces with and without the effects of the control action. Analogously, Fig. 11 reports the end-effector rotations. From these figures, the control action demonstrates to be effective in the achievement of the isotropic compliance property, showing the ability to maintain the parallelism between the prescribed and the target paths and preventing any undesired rotation.

8 Conclusions

In this paper, the isotropic compliance property has been investigated in the Special Euclidean Group SE(3), considering serial redundant manipulators. The solution of the redundancy problem is based on the QR decomposition of the transpose of the Jacobian matrix. The determined control stiffness matrices allow the control system to minimize the work of the joint control torques retaining the isotropic compliance property. Multibody dynamic simulations have been performed by implementing the developed method. Results confirm the feasibility of the proposed approach in manipulators with different degree of redundancy and for prescribed tasks.

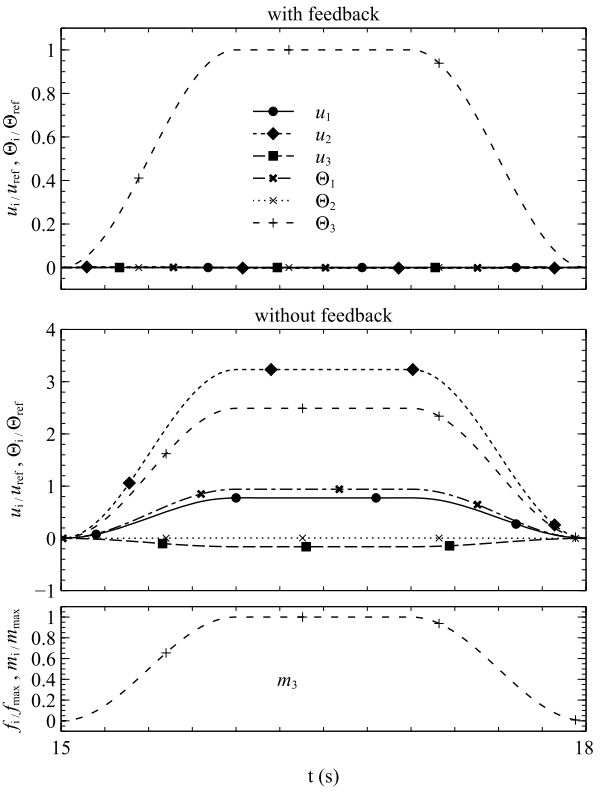

Fig. 15 Seven-DoF manipulator in the posture $\boldsymbol{q}_a$: end-effector displacements and rotations, with and without control action, for the simulation time from 15 s to 18 s (moment applied in the z-axis direction)

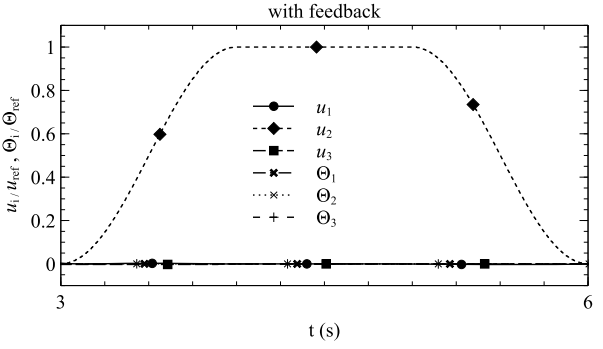

Fig. 16 Seven-DoF manipulator in the posture $\boldsymbol{q}_b$: end-effector displacements and rotations, with and without control action, for the simulation time from 3 s to 6 s (force applied in the y-axis direction)

Appendix

The first posture ($\boldsymbol{q}_a$) end-effector response, in the case of a force applied along the y direction with and without control action, is reported in Fig. 12. Analogously, the cases regarding the force on the z direction, the moment about the x direction, and the moment about the z direction are reported in Fig. 13, Fig. 14, and Fig. 15, respectively. The correspondent end-effector responses for the second case ($\boldsymbol{q}_b$) are reported in Fig. 16, Fig. 17, Fig. 18 and Fig. 19.

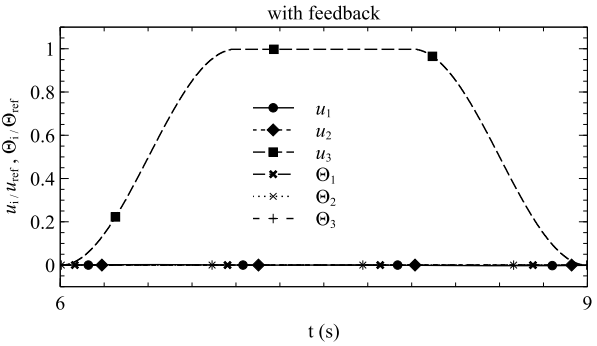

Fig. 17 Seven-DoF manipulator in the posture $\boldsymbol{q}_b$: end-effector displacements and rotations, with and without control action, for the simulation time from 6 s to 9 s (force applied in the z-axis direction)

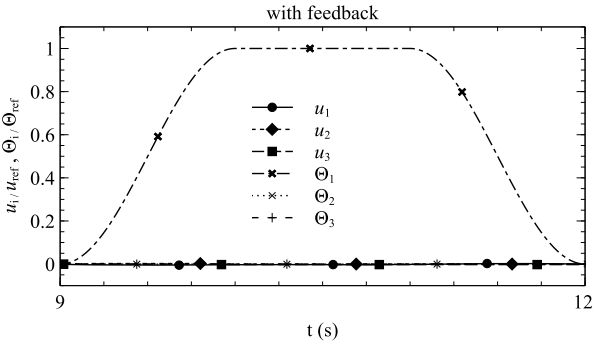

Fig. 18 Seven-DoF manipulator in the posture $\boldsymbol{q}_b$: end-effector displacements and rotations, with and without control action, for the simulation time from 9 s to 12 s (moment applied in the x-axis direction)

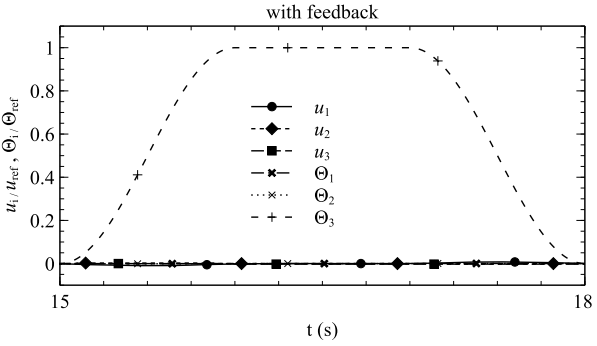

Fig. 19 Seven-DoF manipulator in the posture $\boldsymbol{q}_b$: end-effector displacements and rotations, with and without control action, for the simulation time from 15 s to 18 s (moment applied in the z-axis direction)

References

1. Vinogradov, I.B., Kobrinski, A.E., Stepanenko, Y.E., Tives, L.T.: Details of kinematics of manipulators with the method of volumes. Mekhanika Mashin **1**(5), 5–16 (1971)
2. Klein, C.A., Blaho, B.E.: Dexterity measures for the design and control of kinematically redundant manipulators. Int. J. Robot. Res. **6**(2), 72 (1987)
3. Kumar, A., Waldron, K.J.: The workspace of a mechanical manipulator. J. Mech. Des. **103**, 665–672 (1981)
4. Park, F.C., Brockett, R.W.: Kinematic dexterity of robotic mechanisms. Int. J. Robot. Res. **13**(1), 1–15 (1994)
5. Yang, D.C., Lai, Z.C.: On the conditioning of robotic manipulators - service angle. ASME J. Mech. Transm. Autom. Des. **107**(5), 262–270 (1985)

6. Angeles, J., López-Cajún, C.S.: Kinematic isotropy and the conditioning index of serial robotic manipulators. Int. J. Robot. Res. **11**(6), 560–571 (1992)
7. Yoshikawa, T.: Manipulability of robotic mechanisms. Int. J. Robot. Res. **4**(2), 3–9 (1985)
8. Salisbury, J.K., Craig, J.J.: Articulated hands: force control and kinematic issues. Int. J. Robot. Res. **1**(1), 4–17 (1982)
9. Merlet, J.P.: Jacobian, manipulability, condition number, and accuracy of parallel robots. J. Mech. Des. **128**(1), 199–206 (2006)
10. Bandyopadhyay, S., Ghosal, A.: An algebraic formulation of kinematic isotropy and design of isotropic 6–6 stewart platform manipulators. Mech. Mach. Theory **43**(5), 591–616 (2008)
11. Legnani, G., Tosi, D., Fassi, I., Giberti, H., Cinquemani, S.: The point of isotropy and other properties of serial and parallel manipulators. Mech. Mach. Theory **45**(10), 1407–1423 (2010)
12. Belfiore, N., Di Giamberardino, P., Rudas, I., Verotti, M.: Isotropy in any RR planar dyad under active joint stiffness regulation. Int. J. Mech. Control **12**(1), 75–81 (2011)
13. Belfiore, N.P., Verotti, M., Di Giamberardino, P., Rudas, I.J.: Active joint stiffness regulation to achieve isotropic compliance in the Euclidean space. J. Mech. Robot. **4**(4), 041010 (2012)
14. Angeles, J.: Fundamentals of Robotic Mechanical Systems: Theory, Methods, and Algorithms, vol. 124. Springer, New York (2013)
15. Verotti, M., Belfiore, N.P.: Isotropic compliance in E(3): feasibility and workspace mapping. J. Mech. Robot. **8**(6), 061005 (2016)
16. Verotti, M., Masarati, P., Morandini, M., Belfiore, N.: Isotropic compliance in the Special Euclidean Group SE(3). Mech. Mach. Theory **98**, 263–281 (2016)
17. Calanca, A., Muradore, R., Fiorini, P.: A review of algorithms for compliant control of stiff and fixed-compliance robots. IEEE/ASME Trans. Mechatron. **21**(2), 613–624 (2016)
18. Firouzeh, A., Paik, J.: Grasp mode and compliance control of an underactuated origami gripper using adjustable stiffness joints. IEEE/ASME Trans. Mechatron. **22**(5), 2165–2173 (2017)
19. Verotti, M., Dochshanov, A., Belfiore, N.: Compliance synthesis of CSFH MEMS-based microgrippers. J. Mech. Des., Trans. ASME **139**(2), 022301 (2017)
20. Nasiri, R., Khoramshahi, M., Shushtari, M., Ahmadabadi, M.: Adaptation in variable parallel compliance: towards energy efficiency in cyclic tasks. IEEE/ASME Trans. Mechatron. **22**(2), 1059–1070 (2017)
21. Lee, G., Park, S., Lee, D., Park, F., Jeong, J., Kim, J.: Minimizing energy consumption of parallel mechanisms via redundant actuation. IEEE/ASME Trans. Mechatron. **20**(6), 2805–2812 (2015)
22. Colbaugh, R., Seraji, H., Glass, K.: Obstacle avoidance for redundant robots using configuration control. J. Field Robot. **6**(6), 721–744 (1989)
23. Duguleana, M., Barbuceanu, F.G., Teirelbar, A., Mogan, G.: Obstacle avoidance of redundant manipulators using neural networks based reinforcement learning. Robot. Comput.-Integr. Manuf. **28**(2), 132–146 (2012)
24. Menon, M.S., Ravi, V., Ghosal, A.: Trajectory planning and obstacle avoidance for hyper-redundant serial robots. J. Mech. Robot. **9**(4), 041010 (2017)
25. Zhang, Z., Zheng, L., Yu, J., Li, Y., Yu, Z.: Three recurrent neural networks and three numerical methods for solving a repetitive motion planning scheme of redundant robot manipulators. IEEE/ASME Trans. Mechatron. **22**(3), 1423–1434 (2017)
26. Antonelli, G., Chiaverini, S., Fusco, G.: A new on-line algorithm for inverse kinematics of robot manipulators ensuring path tracking capability under joint limits. IEEE Trans. Robot. Autom. **19**(1), 162–167 (2003)
27. Xiang, J., Zhong, C., Wei, W.: General-weighted least-norm control for redundant manipulators. IEEE Trans. Robot. **26**(4), 660–669 (2010)
28. Flacco, F., De Luca, A., Khatib, O.: Control of redundant robots under hard joint constraints: saturation in the null space. IEEE Trans. Robot. **31**(3), 637–654 (2015)
29. Chiaverini, S.: Singularity-robust task-priority redundancy resolution for real-time kinematic control of robot manipulators. IEEE Trans. Robot. Autom. **13**(3), 398–410 (1997)
30. Fang, J., Mei, T., Zhao, J., Li, T.: A dual-mode online optimization method for trajectory tracking of redundant manipulators. Ind. Robot: An International Journal **43**(2), 241–252 (2016)
31. Vukobratovic, M., Kircanski, M.: A dynamic approach to nominal trajectory synthesis for redundant manipulators. IEEE Trans. Syst. Man Cybern. **4**, 580–586 (1984)
32. Hirakawa, A.R., Kawamura, A.: Trajectory planning of redundant manipulators for minimum energy consumption without matrix inversion. In: Robotics and Automation, 1997. IEEE International Conference on Proceedings, vol. 3, pp. 2415–2420. IEEE, Albuquerque, NM, USA (1997)
33. Halevi, Y., Carpanzano, E., Montalbano, G.: Minimum energy control of redundant linear manipulators. J. Dyn. Syst. Meas. Control **136**(5), 051016 (2014)

34. Hollerbach, J., Suh, K.: Redundancy resolution of manipulators through torque optimization. IEEE J. Robot. Autom. **3**(4), 308–316 (1987)
35. Kang, H.J., Freeman, R.A.: Null space damping method for local joint torque optimization of redundant manipulators. J. Field Robot. **10**(2), 249–270 (1993)
36. Chung, C., Lee, B.H., Kim, M., Lee, C.: Torque optimizing control with singularity-robustness for kinematically redundant robots. J. Intell. Robot. Syst. **28**(3), 231–258 (2000)
37. Fang, J., Zhao, J., Mei, T., Chen, J.: Online optimization scheme with dual-mode controller for redundancy-resolution with torque constraints. Robot. Comput.-Integr. Manuf. **40**, 44–54 (2016)
38. Shin, H., Lee, S., Jeong, J., Kim, J.: Antagonistic stiffness optimization of redundantly actuated parallel manipulators in a predefined workspace. IEEE/ASME Trans. Mechatron. **18**(3), 1161–1169 (2013)
39. Nemec, B., Zlajpah, L.: Force control of redundant robots in unstructured environment. IEEE Trans. Ind. Electron. **49**(1), 233–240 (2002)
40. Nenchev, D., Okawa, R., Sone, H.: Task-space dynamics and motion/force control of fixed-base manipulators under reaction null-space-based redundancy resolution. Robotica **34**(12), 2860–2877 (2016)
41. Ajoudani, A., Tsagarakis, N., Bicchi, A.: Choosing poses for force and stiffness control. IEEE Trans. Robot. **33**(6), 1483–1490 (2017)
42. Masarati, P.: Computed torque control of redundant manipulators using general-purpose software in real-time. Multibody Syst. Dyn. **32**(4), 403–428 (2014)
43. Lin, Z., Patel, R.V., Balafoutis, C.A.: Impact reduction for redundant manipulators using augmented impedance control. J. Field Robot. **12**(5), 301–313 (1995)
44. Kim, K.H., Park, I.J., Choi, J.H., Rhim, S.: Evaluation of head-collision safety of a 7-dof manipulator according to posture variation. Multibody Syst. Dyn. **37**(1), 95–105 (2016)
45. Siciliano, B.: Kinematic control of redundant robot manipulators: a tutorial. J. Intell. Robot. Syst. **3**(3), 201–212 (1990)
46. Zhang, Z., Chen, S., Li, S.: Compatible convex-nonconvex constrained qp-based dual neural networks for motion planning of redundant robot manipulators. IEEE Trans. Control Syst. Technol. **99**, 1–9 (2018)
47. Whitney, D.E.: Resolved motion rate control of manipulators and human prostheses. IEEE Trans. Man-Mach. Syst. **10**(2), 47–53 (1969)
48. Wampler, C.W.: Manipulator inverse kinematic solutions based on vector formulations and damped least-squares methods. IEEE Trans. Syst. Man Cybern. **16**(1), 93–101 (1986)
49. Sciavicco, L., Siciliano, B.: A solution algorithm to the inverse kinematic problem for redundant manipulators. IEEE J. Robot. Autom. **4**(4), 403–410 (1988)
50. Patel, R.V., Shadpey, F.: Control of Redundant Robot Manipulators: Theory and Experiments, vol. 316. Springer, Berlin (2005)
51. Chiacchio, P., Chiaverini, S., Sciavicco, L., Siciliano, B.: Closed-loop inverse kinematics schemes for constrained redundant manipulators with task space augmentation and task priority strategy. Int. J. Robot. Res. **10**(4), 410–425 (1991)
52. Wampler, C.: Inverse kinematic functions for redundant manipulators. In: 1987 IEEE International Conference on Robotics and Automation. Proceedings, vol. 4, pp. 610–617. IEEE, Raleigh, NC, USA (1987)
53. Zhang, Z., Fu, T., Yan, Z., Jin, L., Xiao, L., Sun, Y., Yu, Z., Li, Y.: A varying-parameter convergent-differential neural network for solving joint-angular-drift problems of redundant robot manipulators. IEEE/ASME Trans. Mechatron. **23**(2), 679–689 (2018)
54. Zhang, Z., Lin, Y., Li, S., Li, Y., Yu, Z., Luo, Y.: Tricriteria optimization-coordination motion of dual-redundant-robot manipulators for complex path planning. IEEE Trans. Control Syst. Technol. **26**(4), 1345–1357 (2018)
55. Merlini, T., Morandini, M.: The helicoidal modeling in computational finite elasticity. Part I: variational formulation. Int. J. Solids Struct. **41**(18–19), 5351–5381 (2004)
56. Golub, G.H., Van Loan, C.F.: Matrix Computations. forth JHU Press, Baltimore (2013)
57. Masarati, P., Morandini, M., Mantegazza, P.: An efficient formulation for general-purpose multibody/multiphysics analysis. J. Comput. Nonlinear Dyn. **9**(4), 041001 (2014)